AD-A116 327   NAVAL RESEARCH LAB WASHINGTON DC   F/6 10/2
                NUMERICAL STUDY OF ELECTRON LEAKAGE POWER LOSS IN A TRI-PLATE T--ETC(U)
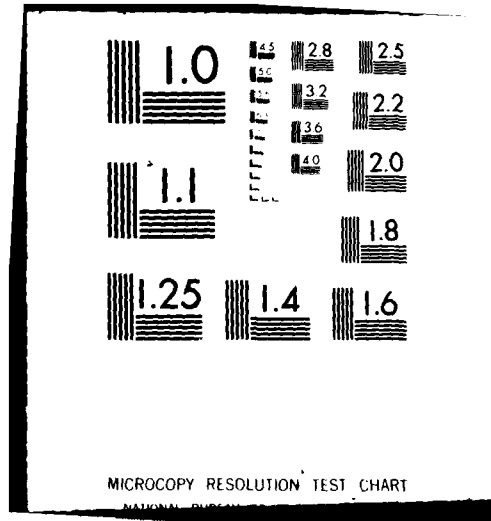   JUN 82   R J BARKER, S A GOLDSTEIN
UNCLASSIFIED   NRL-MR-4837   NL

END
DATE
FILMED
7-82
DTIC

MICROCOPY RESOLUTION TEST CHART

REPORT DOCUMENTATION PAGE		READ INSTRUCTIONS BEFORE COMPLETING FORM
1. REPORT NUMBER NRL Memorandum Report 4837	2. GOVT ACCESSION NO. AD-A116 327	3. RECIPIENT'S CATALOG NUMBER
4. TITLE *(and Subtitle)* NUMERICAL STUDY OF ELECTRON LEAKAGE POWER LOSS IN A TRI-PLATE TRANSMISSION LINE		5. TYPE OF REPORT & PERIOD COVERED Interim report on a continuing NRL problem.
		6. PERFORMING ORG. REPORT NUMBER
7. AUTHOR(s) R.J. Barker* and Shyke A. Goldstein*		8. CONTRACT OR GRANT NUMBER(s)
9. PERFORMING ORGANIZATION NAME AND ADDRESS Naval Research Laboratory Washington, DC 20375		10. PROGRAM ELEMENT, PROJECT, TASK AREA & WORK UNIT NUMBERS DE-AI08-79DP40092; 47-0879-0-2
11. CONTROLLING OFFICE NAME AND ADDRESS Department of Energy Washington, DC 20545		12. REPORT DATE June 23, 1982
		13. NUMBER OF PAGES 34
14. MONITORING AGENCY NAME & ADDRESS(*if different from Controlling Office*) Sandia National Laboratory Albuquerque, NM 87115		15. SECURITY CLASS. *(of this report)* UNCLASSIFIED
		15a. DECLASSIFICATION/DOWNGRADING SCHEDULE
16. DISTRIBUTION STATEMENT *(of this Report)* Approved for public release; distribution unlimited.		
17. DISTRIBUTION STATEMENT *(of the abstract entered in Block 20, if different from Report)*		
18. SUPPLEMENTARY NOTES *Present address: JAYCOR, Inc., 205 S. Whiting Street, Alexandria, VA 22304 This work was sponsored in part by the U.S. Department of Energy, Washington, DC.		
19. KEY WORDS *(Continue on reverse side if necessary and identify by block number)* Magnetic insulation Numerical simulation Radial diode Power loss		

20. ABSTRACT *(Continue on reverse side if necessary and identify by block number)*

Numerical simulations have been conducted using NRL's DIODE2D computer code to model the steady-state behavior of electron flow in a radial diode and in its adjacent tri-plate transmission line (TTL). Particular attention was paid to the magnitude of the electron current flowing from the cathode to the anode surface in the TTL. A quantitative value for this effective power loss is given. The electron current is restricted mainly to the transition region in the TTL into which there is "seepage" of the B_z that is imposed in the diode gap. This finding highlights the importance of that region to diode designers.
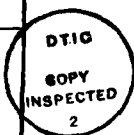
DD $_{1\ JAN\ 73}^{FORM}$ 1473 EDITION OF 1 NOV 65 IS OBSOLETE

S/N 0102-014-6601

CONTENTS

NUMERICAL STUDY OF ELECTRON LEAKAGE POWER LOSS IN A
TRI-PLATE TRANSMISSION LINE

I. INTRODUCTION

There exist two major alternate geometries for intense light ion beam

sources (diodes) to be used in light ion inertial confinement fusion reactor

scenarios. They are the axial pinch-reflex diode (PRD) pioneered at the Naval

Research Laboratory[1] and the magnetically insulated radial diodes under

development at Sandia National Laboratories[2] and Cornell University.[3] Each of

the two diode types have their respective advantages and disadvantages. The

low impedance (0.5-2.0 ohm) PRD's tested on the Gamble II pulsed power

generator at NRL proved themselves capable of delivering over 70% of the net

power flowing through the diodes to the light ion (H^+ and D^+) beams.[4] They

owed their high ion production efficiencies to the theoretically established

benefits of large aspect ratios[5] (cathode radius/A-K gap) and multiple

reflections of electrons through the anode foil.[6] The geometry of the PRD

(pinch-reflex diode) produced an axially flowing ion beam which could then be

directed to illuminate a fusion pellet target located some distance away.[7] In

some current fusion reactor conceptual designs this can be considered an

advantage since the ion beam source could then be located far enough away from

the fusion reactor vessel to protect them from possible radiation and blast

damage. In addition, there would be no limit to the number of individual

axial diode ion beam sources which could be arrayed around a central target to

deliver as much beam power as necessary to the target. Unfortunately,

theoretical analysis has revealed that lower current ion beams lend themselves

more efficiently to transport over multi-meter distances.[8] To maintain a

given power level while boosting transport efficiency, higher impedance ion

diode sources are desirable. Over the past several years NRL has pursued an

experimental ion diode development program under DNA sponsorship at the Harry

Diamond Laboratory (HDL). In that work, diode impedances range from 10 to 40

1

ohms to more closely match the 50 ohm characteristic impedance of the single arm of the AURORA pulsed power generator used there (compared to the 1.5 ohms of NRL'S GAMBLE II). To achieve the higher impedances, lower aspect ratio PRD's were employed and this necessarily lowered the diode's ion production efficiency. Efficiencies of only 20% to 30% were observed.[9, 10] Various techniques are being tested to improve this performance.[11, 12]

Magnetically insulated radial diodes offer a different set of pros and cons. They have been shown to operate at better than 75% ion production efficiency.[13] Since ion flow is focused to the diode centerline, beam transport is not a consideration and low impedances may be employed. This also means that target ignition will take place inside the diode which could result in damage to the device. The power feed geometry for the radial diode may also lead to other difficulties. Figure 1 presents a conceptualization of a possible radial diode test apparatus. As shown in the cutaway view, a large number of individually charged power modules are arrayed around the circumference of the device. They are so designed to dump their stored electrical energy simultaneously into the large disc-like triplate transmission line (TTL) which fills the central portion of the machine. This triplate consists of an anode disc sandwiched between two equispaced cathode discs. The interplate separation may also vary with radius. The TTL (triplate transmission line) terminates in the center with an azimuthally-symmetric radial diode. A possible configuration for that central region is illustrated in Figure 2. The symmetry of the power flow to such a diode is one key consideration.[14] Another is the highly inductive character of the TTL itself. This high inductance can cause a severe lowering (via L . dI/dt) of the voltage across the diode as compared to the voltage output of the individual pulsed power modules. Furthermore, the resistance divided by the
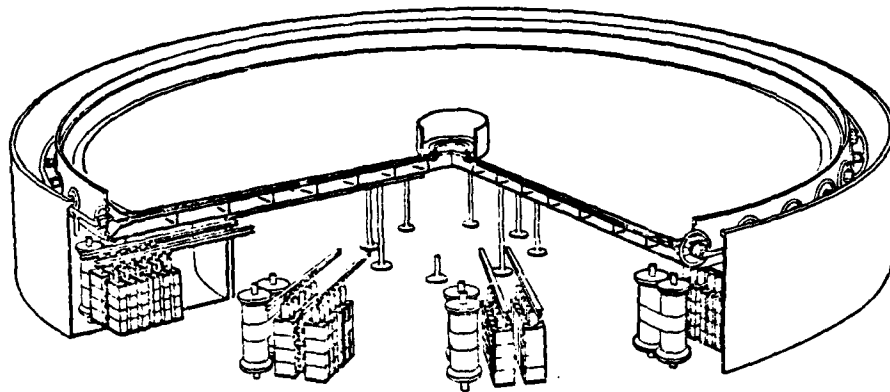
Fig. 1 — Conceptual reactor configuration using tri-plate transmission line and radial diode (courtesy, Sandia Laboratories)
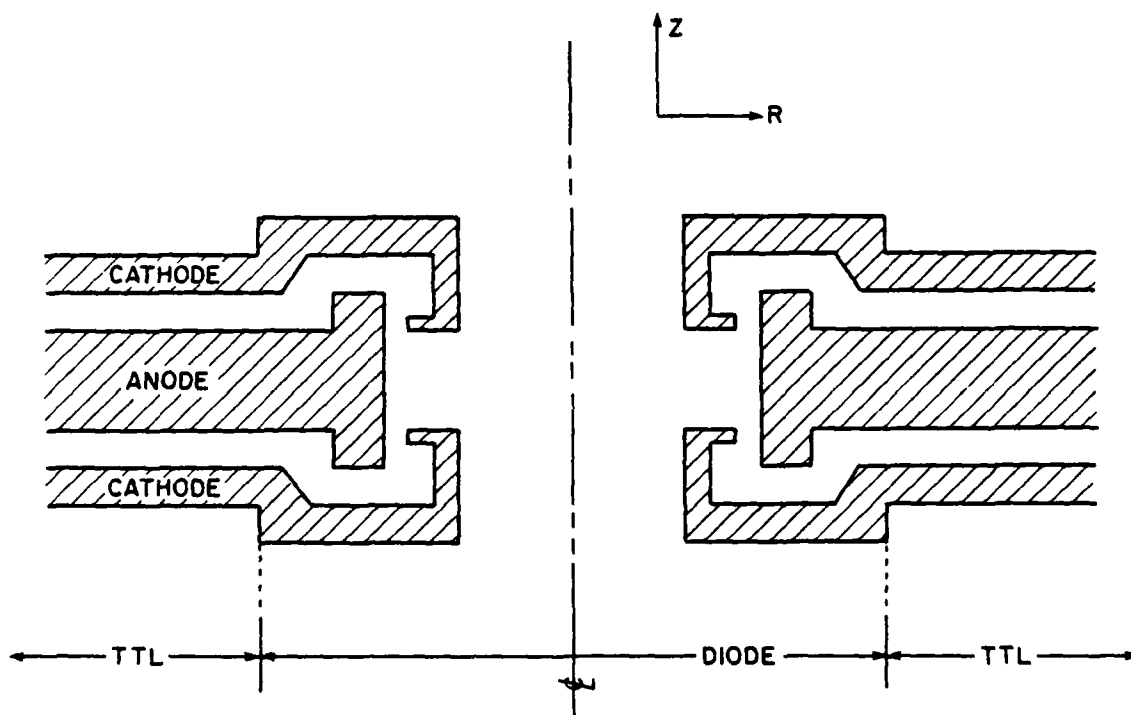

Fig. 2 — Central region of the reactor configuration

inductance of the TTL circuit can lead to a phase shift between the peak voltage across the diode and the peak current flowing through the diode, with unfortunate consequences for the power characteristics of the device. Those problems have been and are being studied elsewhere. This report focuses on yet another possible TTL power loss mechanism, namely that of direct electron flow through the vacuum gap between the plates. The properties of magnetic insulation are well enough understood to ensure that an adequately insulated TTL could be designed with sufficiently large gap spacings for known values of diode current and voltage. However, there is likely to be a transition region in the TTL in the immediate vicinity of the radial diode into which will seep a finite value of the axial magnetic field imposed in the diode's A-K gap. The physics of electron flow in such a transition region cannot readily be dealt with by analytic treatment. For that purpose, this numerical simulation was undertaken.

II. THE RADIAL DIODE AND TTL

The ideal diode and triplate transmission line geometry chosen for analysis is depicted in Figure 3 (drawn to scale). The cathode consists of a solid shank 5.0 centimeters in diameter and 6.4 centimeters long sandwiched axially between two infinite parallel plates. The anode takes the form of a flat annular collar, mounted symmetrically and coaxially to the cathode shank. The anode's inside diameter of 5.5 centimeters yields a radial anode-cathode gap of 0.5 centimeter while its 4.4 centimeter thickness allows a clearance of 1.0 centimeter from each of the parallel cathode plates. An electrical potential difference of 2.0 megavolts is maintained between the electrodes. In addition, a field coil structure is assumed such that a constant and uniform background B_{zo} of 20.0 kilogauss permeates the diode gap
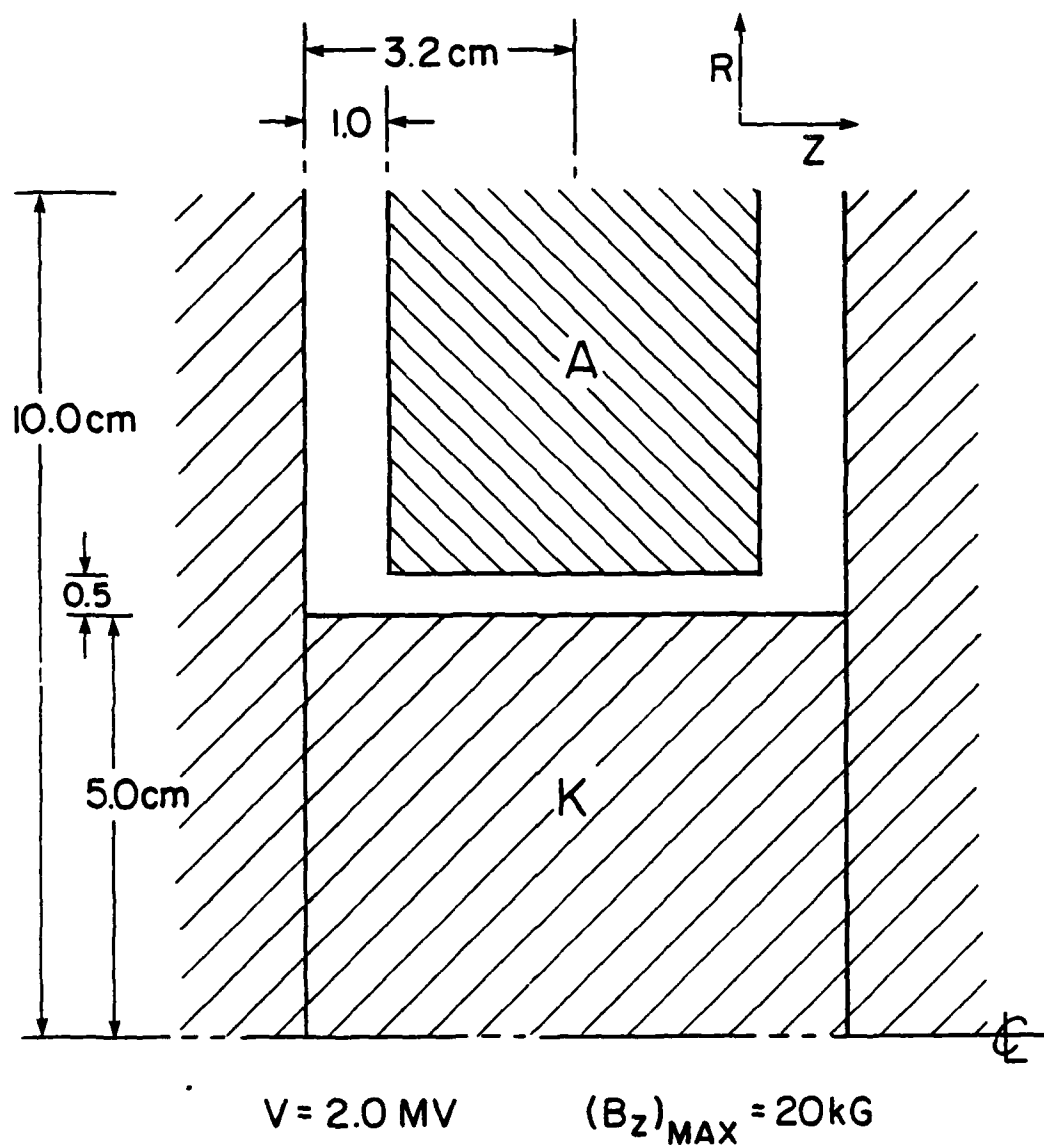
4

Fig. 3 — The radial diode and TTL modeled

completely from R = 5.0 to R = 5.5 centimeter. This field is further assumed to decrease in strength linearly with increasing radius inside the adjacent TTL, until it reaches zero at R = 6.5 cm.

The geometry under consideration may be subdivided into three separate gap regions as shown in Figure 4. Each half of the "infinite" triplate shall be called Region I. It is primarily the diode current flowing axially through the cathode shank which generates an azimuthal magnetic field in this region to insulate the electron flow. Region II consists of the radial anode-cathode gap which is the heart of the radial diode. There too an insulating B_θ arises from the cathode shank current. Note, however, that I_z must go to zero at the diode's center plane. B_θ must vanish with it there. For that reason, it is the strong applied axial magnetic field, B_{zo}, which must be relied upon to insulate the electrons in the diode. The azimuthal field component there serves primarily to complicate the electron flow. Finally, there is the transition volume of Region III. In the lower third of that region, $\vec{B}$ will closely resemble that of II but $\vec{E}$ will be weaker and no longer totally radial. In the upper two-thirds there is a fairly sharp B_z gradient which should act to prevent any TTL electrons from entering II. Exactly where those reflected electrons go is the central question treated herein. Before plunging into the numerics, it is first illuminating to derive some zeroeth-order predictions for Region I and II from simple analytic theory.

Throughout most of Region II, the vacuum electric field has a uniform value of $(E_r, E_z) = (1.33 \times 10^4, 0.0)$ statvolts/cm, while in $(E_r, E_z) = (0.0, 0.666 \times 10^4)$ statv/cm. In the absence of B_z and B_θ in II, the expected space-charge limited electron flow (ignoring ions) may be approximated by the Langmuir-Compton[15] expression
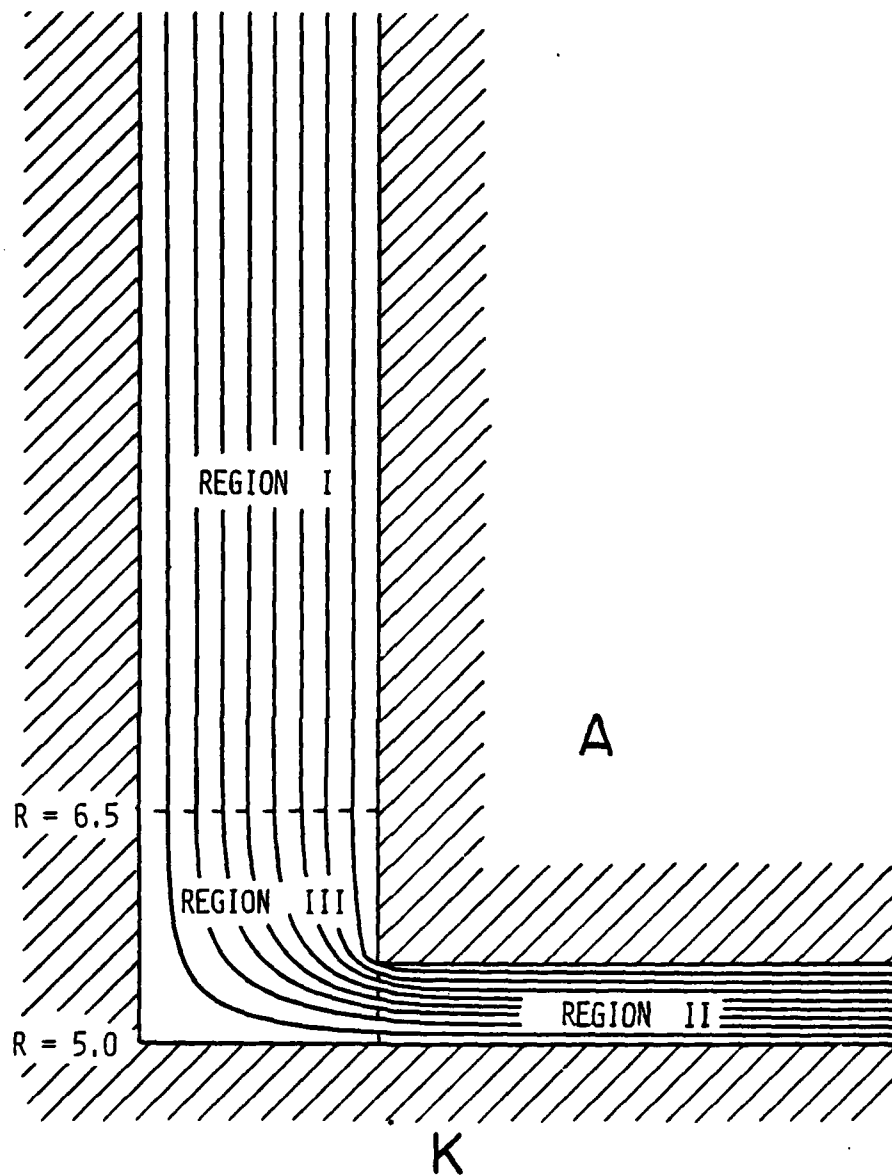
Fig. 4 — The three major regions under study

$$I_e = 14.7 \times 10^{-6} \frac{L \ V^{3/2}}{r \ \alpha_1^2} \ \text{amps} \tag{1}$$

with $\alpha_1 \equiv \delta - \left(\frac{2}{5}\right) \delta^2 + \left(\frac{11}{120}\right) \delta^3 - \left(\frac{47}{3300}\right) \delta^4 + 0.00168 \ \delta^5 \ldots$ where

$\delta \equiv \ell n \left(\frac{r}{r_e}\right)$, r = collector radius = 5.5 cm, r_e = emitter radius = 5.0 cm,

L = length of emitting shank = 4.4 cm, V = diode voltage = 2.0 MV. For the

given values of radii, δ = 0.09531 and α_1 = 0.09176. This predicts an

electron current of 3.95 megamperes in the radial A-K gap (N.B. - This ignores

those portions of the cathode shank in Region III). Significant electron

emission can also be expected along the parallel cathode side plates of Region

I. The space-charge limited electron current density emitted there can be

approximated from the relativistic expression attributed to Friedlander,

et.al.[16]

$$J_e = 2.72 \times 10^3 \left[\sqrt{\frac{aV}{mc^2} + 1} - 0.8471 \right]^2 d^{-2} \ \text{amps/cm}^2 \tag{2}$$

where d = anode-cathode plate separation = 1.0 cm. For the two megavolts

applied, this predicts J_e = 5.1024 kA/cm^2. In the simulation that follows,

electron emission is permitted on these surfaces between R = 5.2 and R = 9.5

cm. This yields an emission area of 198.6 cm^2 in each TTL or a total diode

feed line electron current of about 2.0 megampere. Ignoring the effects of

magnetic fields, this apparatus as modeled would therefore have a total

electron current of about six megamperes. Substituting an electron-ion bi-

polar curr~ t in the A-K gap raises the figure there by about a factor of 1.86

and thereby boosts the total diode current to about 9.35 megamperes.

In order to gauge the effect of magnetic insulation in Region I a

parallel can be drawn with the analysis of the "critical current" in an

idealized parallel plate axial diode.[17] In that device, the axial current

flow generates an axial magnetic field which causes emitted electrons to bend

toward the center axis. If this B_θ (and therefore this I_z) is large enough,

the electron will not reach the anode plate. Ignoring the effects of the

emitted electron space-charge, a simple estimate can be made for the "critical

current," I_c, necessary to produce an electron trajectory which just grazes

the anode surface:

$$I_c = 8500 \ \beta\gamma \ \left(\frac{R}{d}\right) \text{ amperes} \qquad (3)$$

where R = the radius of emission, d = A-K gap, and β and γ have their standard

relativistic definitions. Here β_{max} = 0.98, γ_{max} = 4.9, and d = 1.0 cm so

that the equation becomes

$$I_c = 4.08 \times 10^4 \text{ R amperes} \qquad (4)$$

The axial current taking part in the physics of Eq. 4 may be considered to

consist only of the total cathode shank current (i.e. - one half of the net

Region II current). By definition, the insulated electron flow in the TTL can

contribute no net axial current. The previous, crude estimate of electrons-

only I_{II} of 3.95 MA leads to an axial current of 1.98 MA which implies, via

Eq. 4, magnetic insulation out to a radius of about 48.5 centimeters.

However, in a properly functioning radial diode, the current prediction of Eq.

1 will not hold true. The relativistic electron gyroradius in the imposed 20

kG axial magnetic field is only 0.41 cm, well below the 0.50 cm width of the

gap. Thus, magnetic insulation should prevail and estimates for diode

performance should be sought directly from the literature on magnetically

9

insulated coaxial charge flow. In one of the most recent comprehensive
treatments on the subject,[18] it was noted that the critical field for
insulation is given by

$$B_c = \frac{mc^2}{e} \left(\frac{2 \, r_A}{r_A^2 - r_c^2} \right) \; (V_0^2 + 2 \, V_0)^{1/2} \qquad (5)$$

where r_A is the anode radius, r_c is the cathode radius
and $V_0 = \frac{e}{mc^2} \phi_0$. For $\phi_0 = 2$ MV, V_0 equals 3.9 and B_c becomes 17 kG, well below
the chosen value of $B_{z0} = 20$ kG in the diode under consideration. There also
appears in Reference 18, rough parametric plots of ion current values for
various combinations of diode characteristics. From those plots, it may be
crudely approximated that the ion current in Region II should be about 2-3
times the Langmuir-Blodgett ion current, I_{LB}. This I_{LB} will be equal to the
previously predicted 3.95 MA for electrons multiplied by the square root of
the electron-proton mass ratio, m_e/m_i. This leads to a Region II ion current
of about 200-300 kA and a half-current of 100-150 kA which in turn implies
magnetic insulation in the TTL out to a radius of only 2.45 to 3.68 cm. This
translates to no insulation at all in the TTL since its lower radius is 5.0
cm. Only the full numerical simulation can accurately show what the true
outcome will be.

III. THE COMPUTATIONAL EXPERIMENT

The numerical simulation of the radial diode was carried out with the
latest version of NRL's DIODE2D computer code.[19] This code is two and one-
half dimensional (i.e., particles are allowed two spatial coordinates, r and
z, as well as three canonical momentum components P_r, P_z and P_θ). The
computational "particles" are azimuthally-symmetric charge/current rings with

charge-to-mass ratios corresponding exactly to that of electrons and protons. The motion of these macroparticles is treated completely relativistically. DIODE2D is a particle-in-cell (PIC) code in which macroparticle charges and current densities are area-weighted over the four nearest grid points on the computational mesh. In its electrostatic, magnetostatic treatment, DIODE2D solves Poisson's equation to obtain $\phi(r,z)$ and $A_\theta(r,z)$ respectively from $\rho(r,z)$ and $J_\theta(r,z)$.[20] From these the self-consistent fields are given by $\vec{E} = -\nabla\phi$ and $\vec{B} = (B_r, B_z)_{self} = \vec{\nabla} \times \vec{A}$. The azimuthal component of the self-magnetic field, B_θ , is found directly through radial integration of Ampere's Law over the mesh. Regularly shaped conductor regions which exclude electric field and magnetic flux may be overlayed on the computational mesh by utilizing a capacitance matrix technique[21] in the Poisson solving algorithm. This optional capability was essential for this particular simulation. A static and spatially non-uniform axial magnetic field is imposed on the computational mesh in a manner presented in the treatment below.

Figure 5 depicts the layout of the computational mesh used to model the combined radial diode and TTL of Figure 4. Due to its left-to-right symmetry, only the left-half of the device is modeled on the computer. Thus, the current values tabulated in Section IV for the numerical model must be multiplied by two to apply to the entire diode. In setting up the computational mesh primary attention was paid to ensuring needed spatial resolution of field and particle motions in all regions of interest. As presented in Section II, the electron gyroradius in the radial gap is approximately 0.41 cm. A minimum of four cells per gyroradius is desired so Δr is fixed at 0.1 cm. Considerations regarding the fast fourier transform technique employed in the Poisson solver allow increased generosity with the
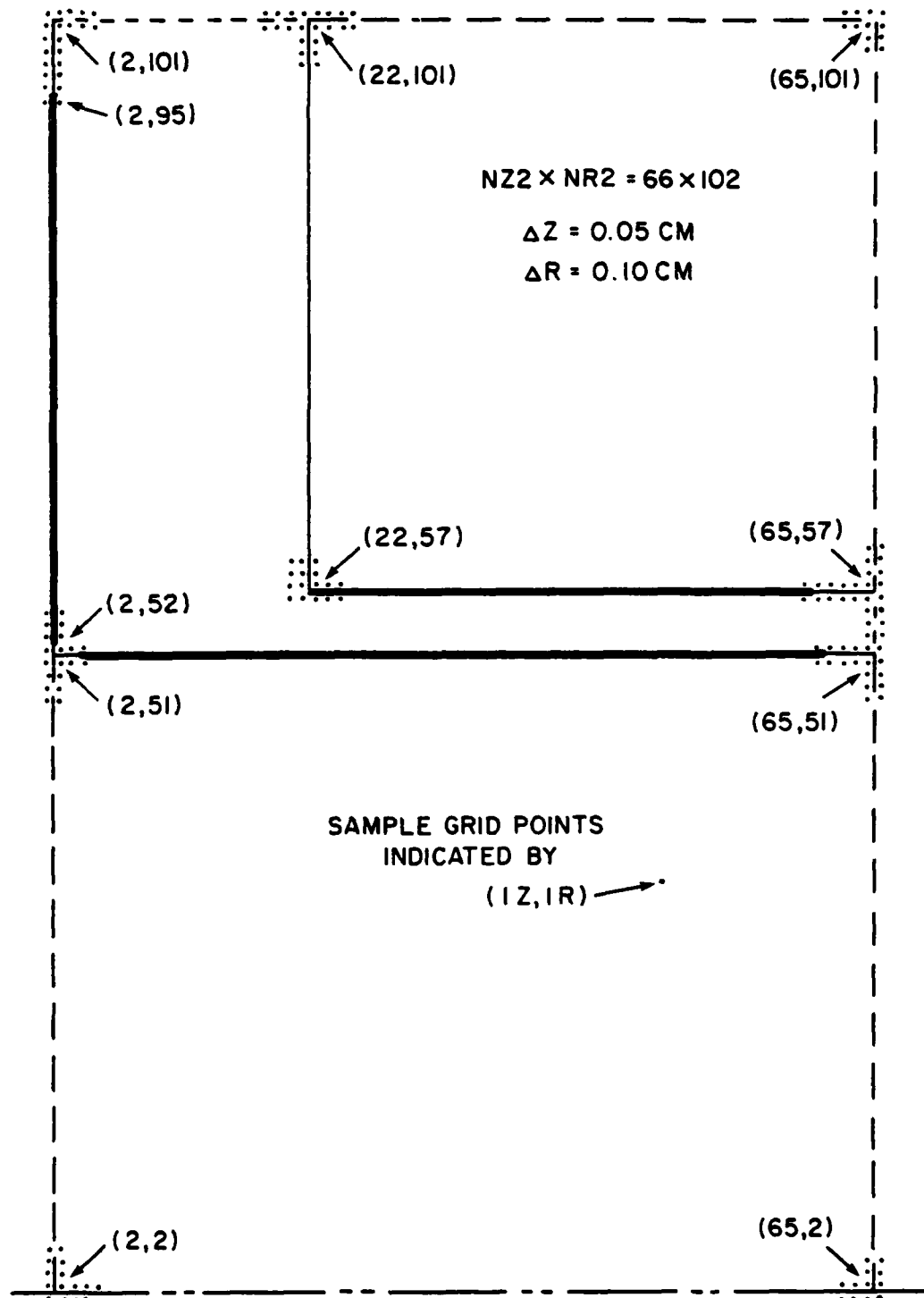
11

(2,101)

(22,101)

(65,101)

(2,95)

NZ2 × NR2 = 66 × 102

ΔZ = 0.05 CM

ΔR = 0.10 CM

(22,57)

(65,57)

(2,52)

(22,57)

(2,51)

(65,51)

SAMPLE GRID POINTS
INDICATED BY

(IZ,IR)

(2,2)

(65,2)

Fig. 5 — Layout of the numerical grid

number of axial gridpoints so that a Δz of 0.05 cm is chosen. For the specified diode dimensions this yields a computational mesh spanning 64 cells in z and 100 cells in r.

The _temporal_ resolution employed in the simulation plays an equally significant role and, if misjudged, may lead to gross numerical instabilities. Once again, the electron gyromotion is a determining factor. Its frequency, f_G, is estimated to be approximately 5.6×10^{10} hertz and proper representation of electron motion demands that $f_G \cdot \Delta t \ll 1.0$. At the same time, it is desirable to follow the simulation through several ion anode-to-cathode crossing times in order to assure that a believable steady state has been reached. For the given voltage of 2 MV, about 1.2×10^{-9} second is consumed by an ion traversing the radial gap. In order to keep the cost of the simulation at a reasonable level, this crossing time should correspond to no more than 1000 timesteps. These upper and lower brackets suggest a timestep of $\Delta t = 2.0 \times 10^{-12}$ second. For this choice, $f_G \Delta t \simeq 0.11$ and the ion crossing time equals 600 timesteps.

Particles are injected into the diode gap using the space charge limited emission condition. (Just enough charge is emitted so that the component of the electric field normal to the emission surface vanishes.) In this simulation, electron emission is permitted up to a radius of 9.5 cm as well as all along the axial cathode surface to within 0.2 cm of the diode center plane. Emission was suppressed at the extrema of the computational mesh because of expected distortion of field values near the boundaries. In contrast ion emission is restricted to the inner axial anode surface except for the region with 0.2 cm of the diode center plane. Emitting sufaces are indicated by the heavy lines in Figure 5. Since only the left half of the

diode is being simulated complete symmetry demands that any particles impacting the right-hand computational boundary are perfectly reflected back into the simulation mesh.

The question of electric and magnetic boundary conditions is not trivial to handle properly. Since no particle emission is permitted closer than 0.5 cm (5 data cells) to the outer radial boundary of the TTL, there is no serious problem in assuming no change to the source-free, static potential solution there during the entire simulation. For that reason, the electrostatic potential, ϕ, rises linearly in z from o to ϕ_0 across the 1 cm gap along that boundary (see Figure 4). (The magnetostatic boundary condition there is irrelevant since there is no B_z imposed in Region I.) The right boundary of Region II is more difficult. It clearly does not remain source-free during the simulation. Unfortunately, the capacitance matrix in the Poisson-solver must be recalculated every time the boundary values of the potentials change. This is a costly procedure. Rather than pay the price of matrix recalculation, it was decided to freeze the values of ϕ along that boundary as well at their source-free, logarithmically-spaced values (as in Figure 4). In addition, no self magnetic flux penetration across that diode centerplane is permitted. These conditions do some violence locally to the $\vec{E}$ and $\vec{B}$ field structure there but the gross dynamics of Region II should remain unaltered.

IV. RESULTS

To better understand the physics of the device, two distinct simulations were conducted. In the first, a benchmark for the radial diode operation was sought by permitting electron emission only on the cathode shank. This provided better estimates for the ideal magnetic insulation to be expected in the TTL region and it gave a reference figure for the maximum operating power

14

of the diode itself. The second simulation allowed electron emission all along the cathode surface in the TTL as well as along the shank. Sample particle position plots were generated to depict the nature of the electron flow there in conjunction with plots of the radial profile of electron current densities striking the anode surface in the TTL. Direct measurement was made of the electron current flowing in Region I to yield the percentage of total power which never reached the diode.

Case I, which simulated only the radial diode, was run over 1200 timesteps of 2.0×10^{-12} second each. The electron and ion currents of the half-diode being modeled are depicted in Figure 6. (Multiply by 2 to obtain full diode currents.) During the first 400 timesteps, only electron (no ions) were permitted in the system. The dots on the plot represent emitted electron current. The solid lines are the collected ion and electron currents as indicated. Note that the electron flow was completely insulated in the diode during electron-only operation. A steady electron current of about 75 kA continued to be emitted by the cathode shank but an equal electron current was continuously absorbed by the shank. This is characteristic of ideal magnetic insulation.[22,23] A constantly replenished cloud of electrons is formed adjacent to the cathode surface and extends some finite radial distance into the A-K gap. This is illustrated in the sample electron position plot of Figure 7. (Note again that only half of the diode is shown. The other half is completely symmetric about the center-plane.) No net current is flowing through the diode. Therefore, the TTL is completely uninsulated. Electrons in that region are free to migrate toward the anode limited only by the self-fields they may generate.

At $T = 400 \Delta t$, ion emission was "turned on" all along the cylindrical anode surface. The resultant neutralization of electron space charge caused a
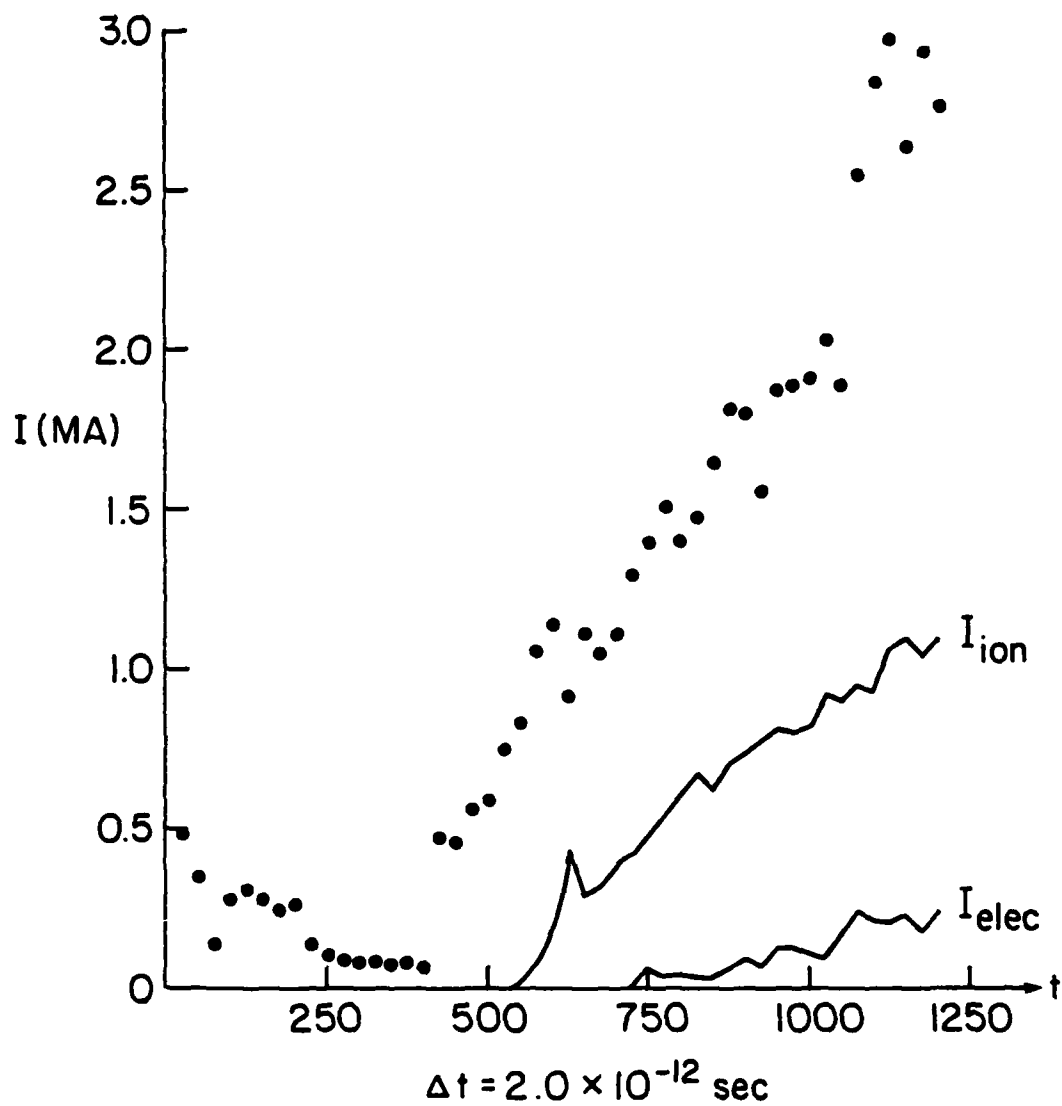
15

Fig. 6 — Electron and ion currents in the radial diode "Benchmark" case
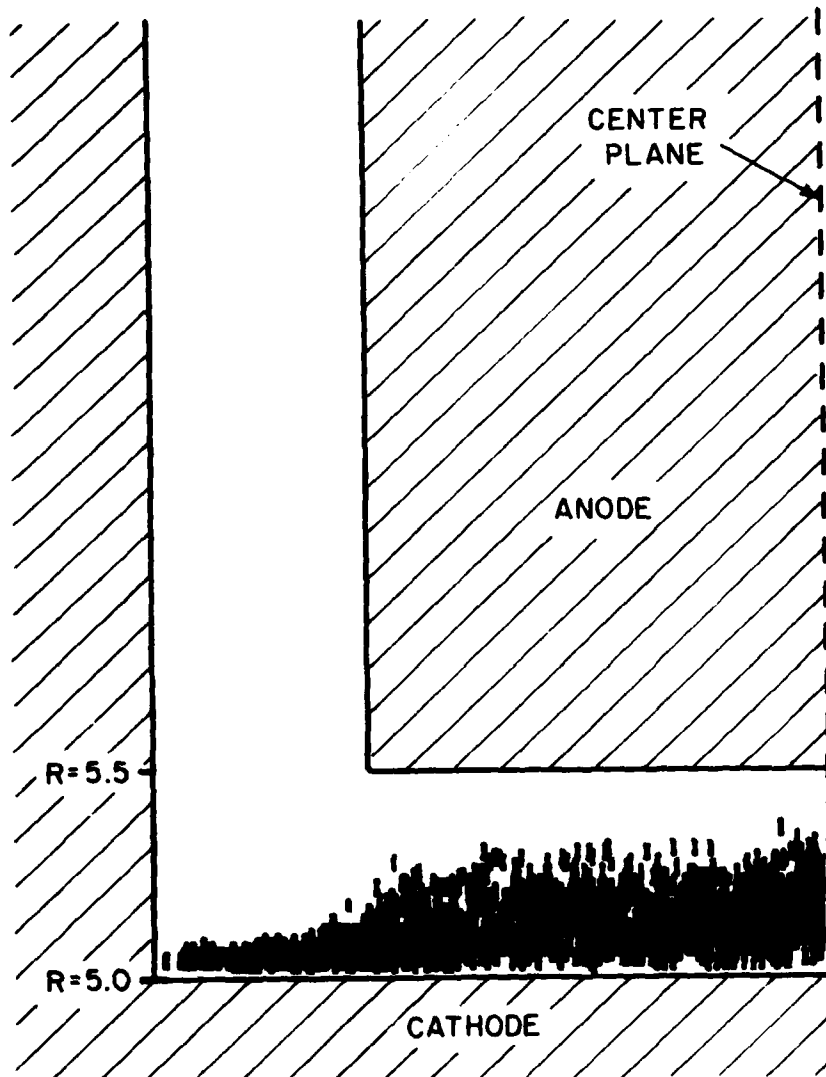
16

Fig. 7 — Sample electron positions with electrons-
only flow in the "Benchmark" case

sharp increase of electron emission as seen in Figure 6. In the new equilibrium state formed by the two-specie flow, almost 3 MA was continuously emitted and reabsorbed by the cathode half-shank to maintain the enlarged negative space-charge cloud depicted in Figure 8. The densest portion of the cloud is now within one millimeter of the anode surface. This accounts for the steady-state ion half-current of about 1.1 MA, far above the simple Langmuir-Blodgett prediction of 100-150 kA. In contrast, the net electron half-current is a mere 250 kA compared to the nearly 2 MA L.-B. estimate. The net current flowing through one-half of the diode is thus about 1.35 MA. According to Eq. 4, this should provide magnetic insulation in the TTL out to a radius of about 33 cm if the imposed axial magnetic field were not present. However, B_z cannot be ignored. It is the key to ion-efficient operation of the radial diode.[24] In combination with the diamagnetic self-fields generated by charge circulation in the electron cloud, the imposed B_z forms an axial magnetic field in the A-K gap whose average radial profile is as shown in Figure 9. The net field gradient is mild in the electrons-only case but exceeds 140 kG/cm when full two-specie flow is present. The field strength peak of almost 70 kG near the anode surface in Region II acts as an effective barrier against electron penetration there. The details of the role this B-field plays in the A-K gap physics is discussed elsewhere.[25] Of primary importance here is the "spill-over" of this field into Region II, the lower end of the TTL.

In the model chosen for this simulation, the imposed 20 kG field is spacially uniform between R=5.0 and R=5.5 cm. It decays linearly to zero with increasing radius between R=5.0 and R=6.0 cm in the TTL. To that background field must be added the particle self-fields. Sample values of the net $B_z(r,z)$ are presented in Figure 10 for the cases with and without ions . Note
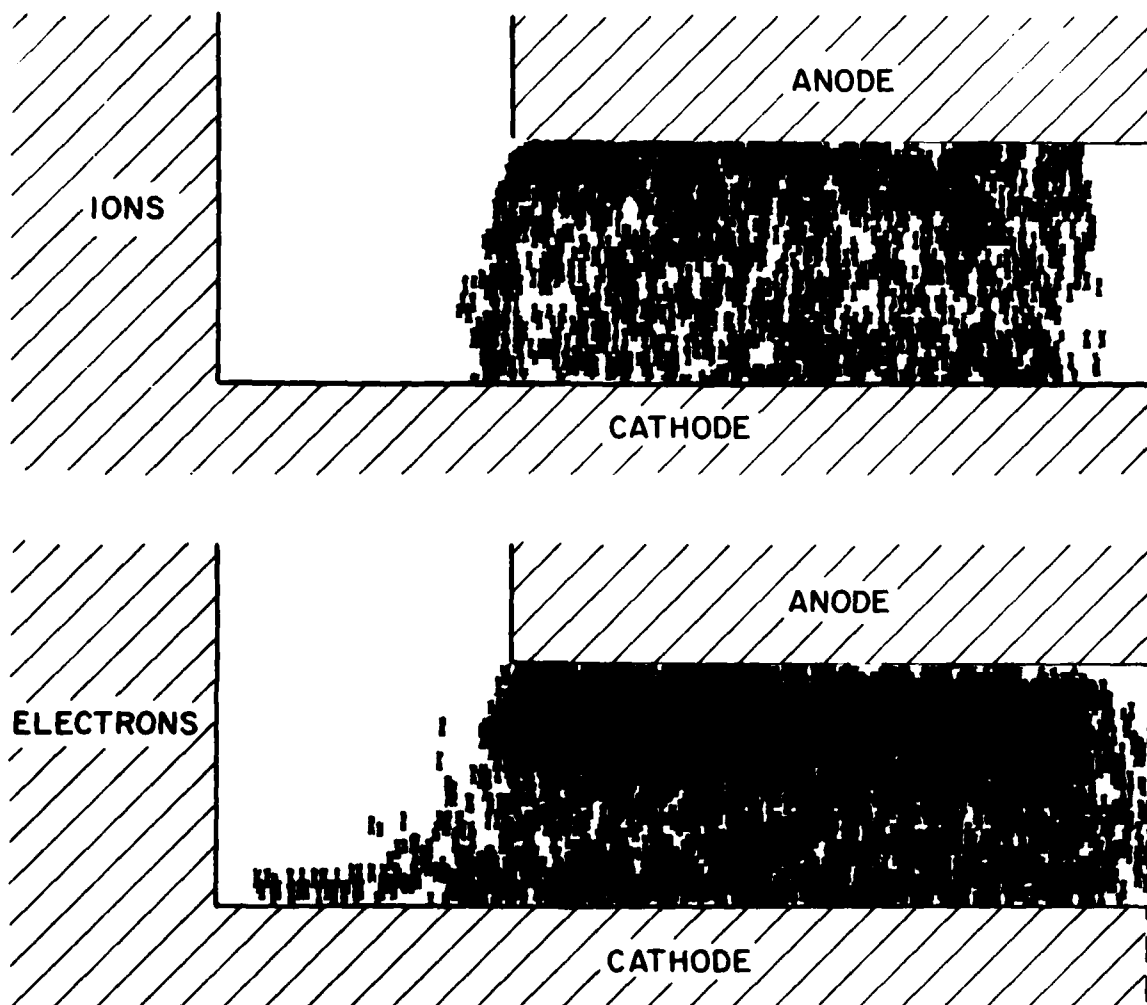
Fig. 8 — Sample ion and electron positions for the full,
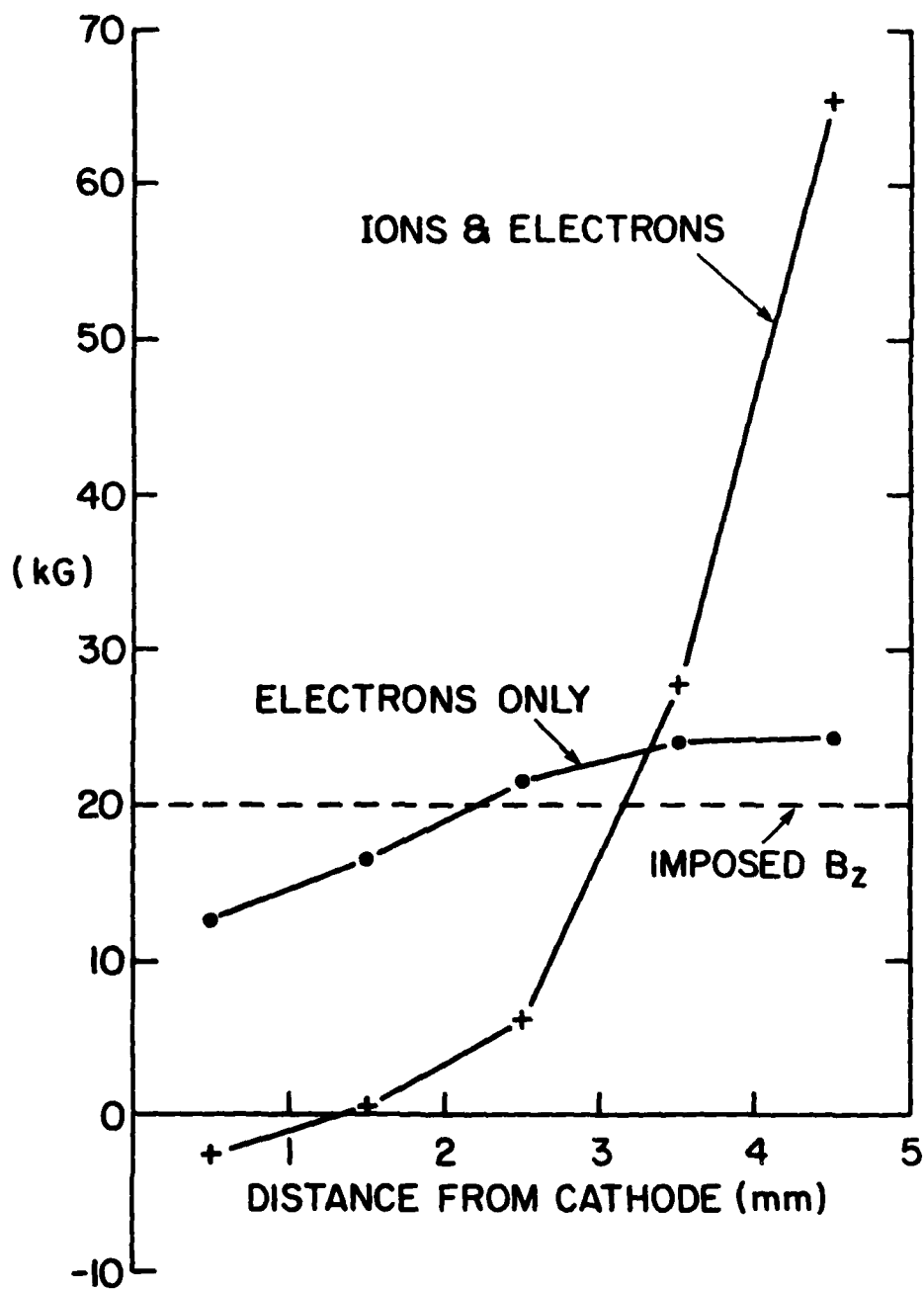equilibrium "Benchmark" case

Fig. 9 — Radial profile of B_z in the A-K gap (averaged in the z = direction) for the "Benchmark" case

```
10.0   10.0   10.0   10.0   10.0
12.0   12.0   12.0   12.0   12.0                          VACUUM    CASE
14.0   14.0   14.0   14.0   14.0
16.0   16.0   16.0   16.0   16.0
18.0   18.0   18.0   18.0   18.0
20.0   20.0   20.0   20.0   20.0   20.0   20.0   20.0   20.0   20.0   20.0   20.0   20.0   20.0   20.0   20.0


10.0   10.0   10.0   10.0   10.0
12.1   12.1   12.1   12.1   12.0
14.0   14.1   14.1   14.1   14.1                       ELECTRONS - ONLY   CASE
16.0   16.1   16.1   16.1   16.1
18.0   18.1   18.1   18.1   18.2
20.0   20.0   20.0   20.1   20.4   21.3   22.2   23.0   23.9   24.7   25.3   25.8   26.4   26.5   25.8   23.6


10.0   10.2   10.4   10.6   10.5
12.1   12.3   12.6   12.9   12.7
14.1   14.3   14.7   15.3   15.3                      ELECTRONS - AND - IONS   CASE
16.1   16.3   16.8   17.8   18.7
18.1   18.2   18.7   20.2   24.1
20.0   20.1   20.4   21.9   28.7   59.2   65.1   69.6   66.8   70.0   74.7   67.9   61.2   64.0   70.9   52.3
```

Fig. 10 — Sample values of B_z near the anode for the
pure radial diode "Benchmark" case

that the Region II fields are hardly modified at all in the electrons-only steady state. The addition of ions into the system, as already pointed out, does make a significant difference. Particularly on the anode side of Region III, the values of B_z are elevated, resulting in a somewhat steeper magnetic gradient. The modification of the fields there, though significant, is quite small in comparison to the tripling of B_z inside Region II. Therefore, it is the imposed field gradient in the TTL that will be responsible for loss of insulation there. Over most of the axial distance, that gradient is little changed by current flows in the diode.

The second simulation run, Case II, tested the full combination of the radial diode and the TTL. Figure 11 provides the corresponding point plot of emitted electron current as well as traces of collected ion and electron currents. Once again, the numerical model was run for the first 400 timesteps without any ions present. The plot shows about 620 kA of electron current continuously emitted in the steady state with a full 450 kA of it being collected by the anode. This leaves about 170 kA of electrons to sustain any recirculating electron cloud in Region II or in the TTL (compared with 75 kA in Case I). The fate of the 450 kA net flow can be deduced from the sample electron position plot of Figure 12. Electrons appear to be bridging the TTL gap out to a radius of about 7.5 centimeters or more. The fact that electrons make it across at all is consistent with the previously determined lack of electron-only current flow across the radial diode gap. Any B_θ insulation in the TTL must therefore arise from the electron current bridging the gap there. A simple estimate may be obtained for the minimum insulation radius by equating the critical current of Eq. 4 with the net TTL current below a
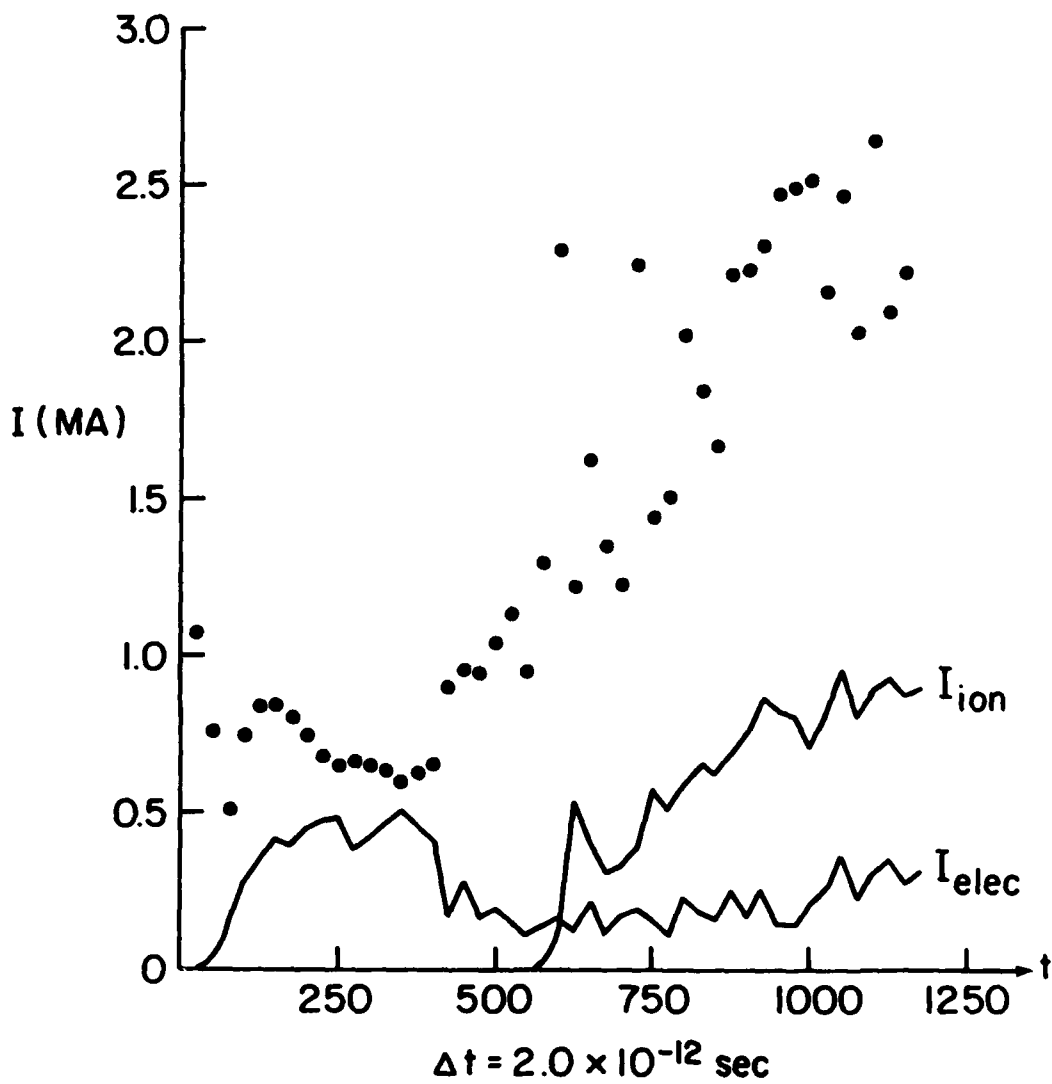
Fig. 11 — Electron and ion currents in the full radial diode-TTL case

Fig. 12 — Sample electron positions with electrons-only flow in
the diode-TTL case

radius, R, assuming a uniform J_e of 5.1 kA/cm^2 as determined from Eq. 2. This produces the expression:

$$\pi \, (r^2 - 5.5^2) \; 5.1 \times 10^3 = 4.08 \times 10^4 \; R \qquad\qquad (6)$$

which yields a minimum radius of about 6.9 centimeters, in agreement with what is observed in the simulation. For a more complete picture of the electron flow pattern in the TTL, the emitted and collected electron current densities, J_e, were plotted in Figure 13. An integration of the collected current yields 425 kA, which accounts for essentially all of the net 450 kA of electron current flowing through the device. Furthermore, the primary peak of collected J_e lies below 6.5 cm in radius in agreement again with the theoretical estimate of 6.9 cm. It is also interesting to note the profile of the emitted j_e. As expected, the highest peak lies above R=9.0 cm where the electron emission region begins and the surface E-fields are highest due to two-dimensional distortions in the equipotential line there. At that high radius, however, the B_θ is more than adequate to prevent the emitted electrons from reaching the anode. They are bent around to strike the cathode again at around R=8.0 cm, causing a virtual shut-off of emission there due to a buildup of negative space-charge. The emission profile is much more steady below R=7.5 cm where B_θ is not strong enough to confine electron flow near the cathode.

As in the previous case which looked only at the radial diode, ion emission in Region II was "turned on" at T=400 Δt. The relaxation of the system to a new steady state can be traced in Figure 11. By T=1200 Δt, the ion half-current collected has settled to about 925 kA while that of the electrons is about 300 kA. Figure 14 depicts a sample set of electron and ion
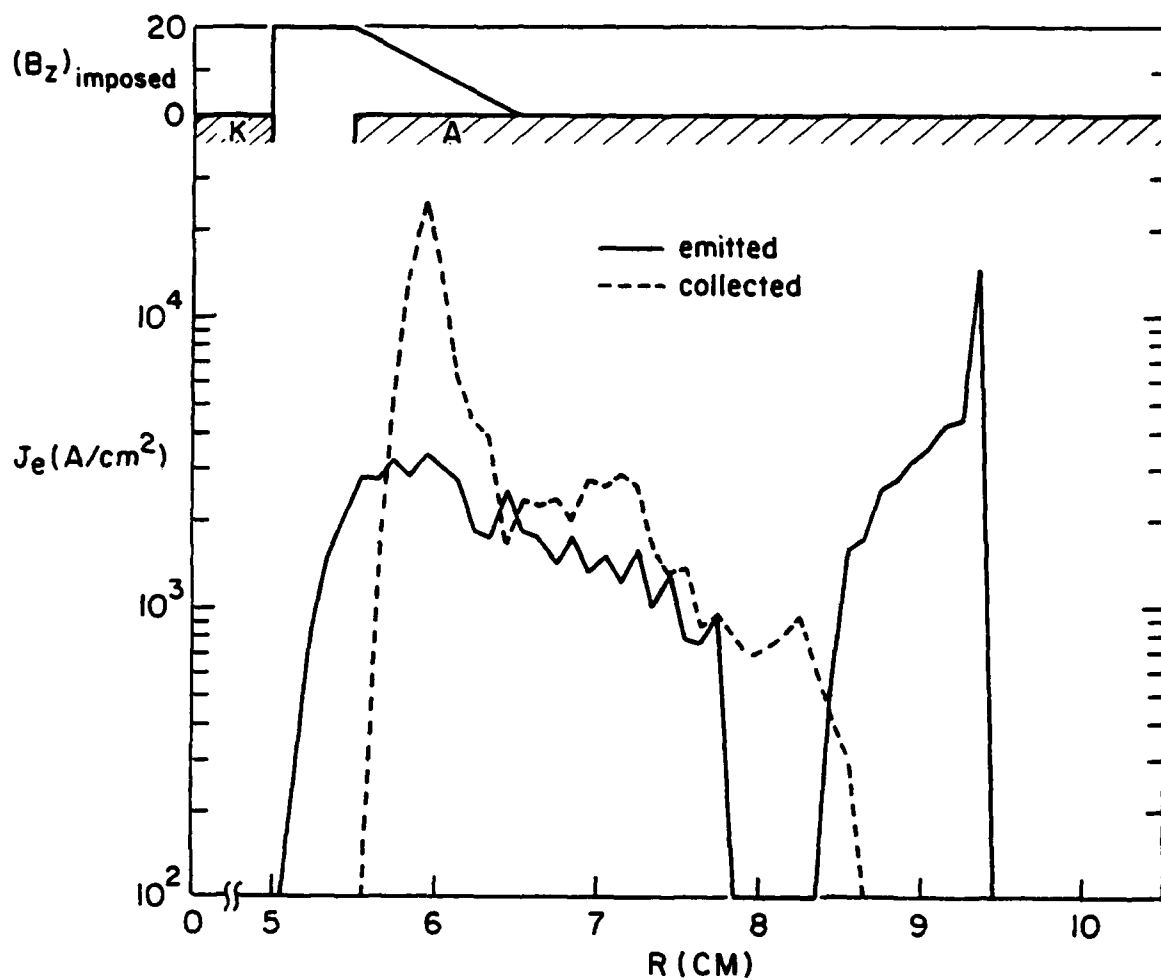
Fig. 13 — Radial profiles of emitted and collected electron current densities in the TTL for electrons-only flow
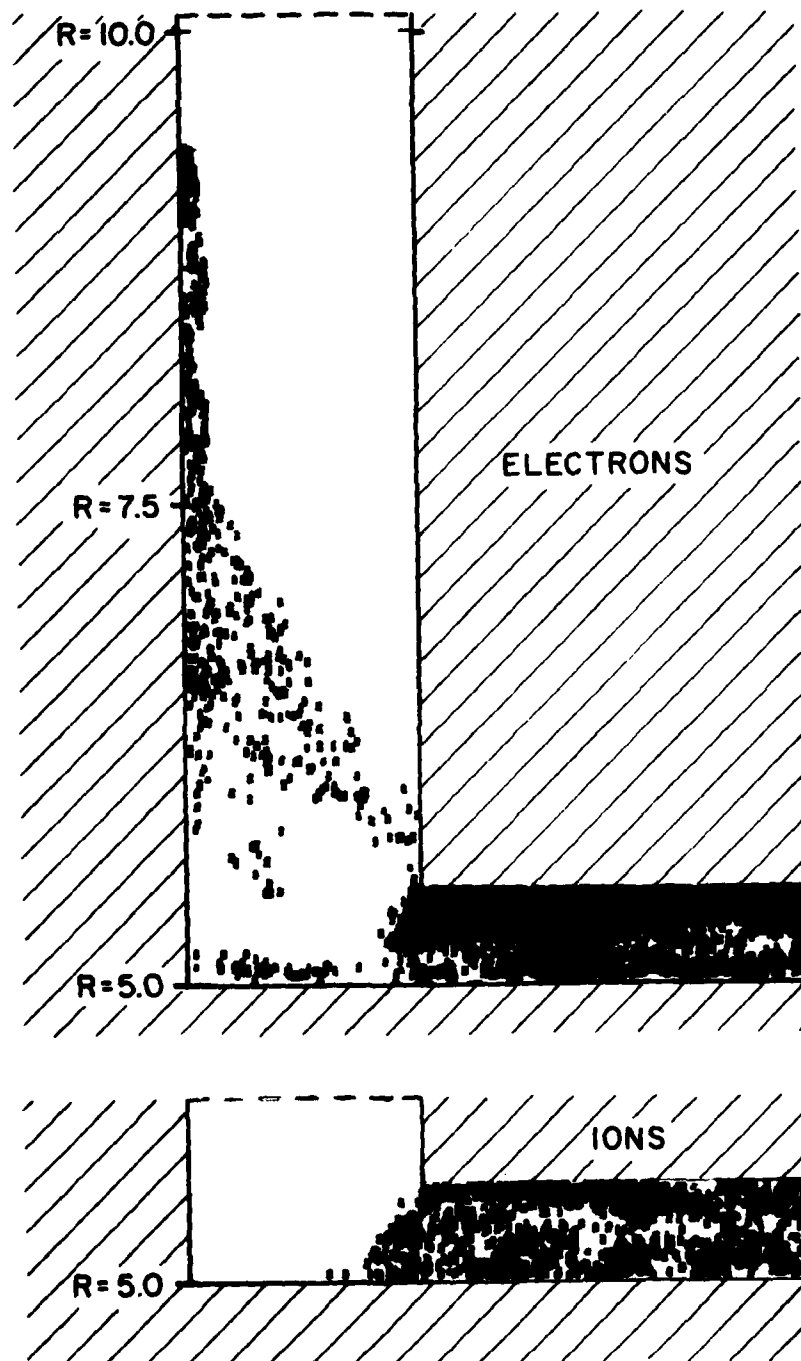
Fig. 14 — Sample ion and electron positions for the full,
equilibrium diode-TTL case

positions at equilibrium. The electron plot is very different from that of Figure 12. As previously stated, an ion half-current of about 1.0 MA is more than adequate to insure magnetic insulation throughout the TTL in the absence of any B_z. Thus it is no surprise to see electrons there confined to a thin sheath near the cathode surface down to about 6.5 cm, where the applied axial B-field begins to rise in value from zero to a full 20 kG at R=5.5 cm. In that annular band between 5.5 and 6.5 cm, a very significant leakage of electron current to the anode occurs. This shorting should not manifest itself were it not for the applied B_z gradient there. To quantify the amount of power lost due to this leakage, the radial profiles of the electron current density emitted and collected in the TTL are plotted in Figure 15. The emission profile is quite irregular. Peaks and troughs alternate down the entire length. Enhanced emission at one point leads to negative charge buildup downstream in the electron sheath, causing reduced emission there. On the other hand, the collected J_e plot consists of a single, intense band below R=6.5 cm as could be guessed from the sample position plot of Figure 14. A total of about 205 kA of electron current is impacting there in the TTL. This corresponds to a full two-thirds of the net electron current flowing through the entire device. What is even more disturbing is that 0.41 terawatts out of a total of 2.45 TW flowing through the half-diode modeled are being lost in the TTL.
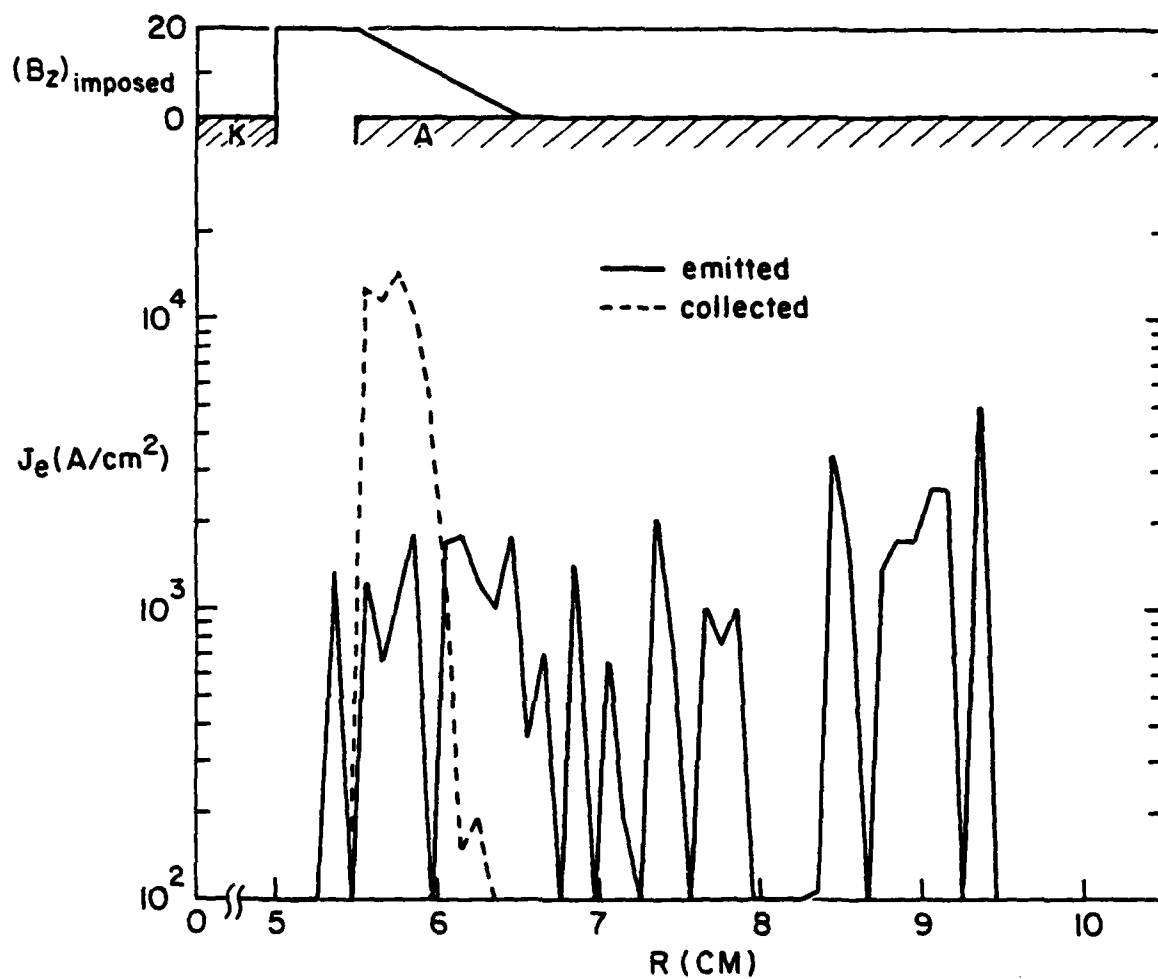
Fig. 15 — Radial profiles of emitted and collected electron current densities
in the TTL for the full diode-TTL case

29

V. CONCLUSIONS

The major findings of this set of numerical simulations are summarized in Table 1. As stated in the introduction, the optimization of net ion production efficiency is a central objective of pulsed power diode research. The table shows a loss of almost 20% of the net input power in the TTL for the configuration modeled. The loss can be attributed to the steep gradient in B_z in the transition region between the TTL and the radial diode. The result is about an 8% drop in the total ion production efficiency of the TTL-diode combination. That can probably be tolerated for most practical applications. However, any experimental configuration different from that shown in Figure 3 will experience a different and possibly greater power loss in the TTL. One must clearly exercise care in setting the TTL gap and in shaping any imposed magnetic field profiles in the transition region.

<div align="center">

Table 1 — Summary of results

</div>

	CASE I		CASE II	
ions present ?	no	yes	no	yes
$(I_e)_{emitted}$	0.15 MA	6.0 MA	1.24 MA	5.0 MA
$(I_e)_{collected\ in\ TTL}$	-	-	0.9 MA	0.4 MA
$(I_e)_{collected\ in\ diode}$	-	0.5 MA	0	0.2 MA
$(I_i)_{collected}$	-	2.2 MA	-	1.85 MA
$\eta_{i_D} = \left(\dfrac{I_i}{I_i + I_e}\right)_D$	-	0.815	-	0.902
$\eta_D = \dfrac{P_D}{P_D + P_{TTL}}$	1.0	1.0	0	0.833
$(\eta_i)_{net} = \eta_{i_D} \cdot \eta_D$	-	0.815	-	0.751

REFERENCES

1   S. J. Stephanakis, D. Mosher, S. A. Goldstein, et.al., Bull. Am. Phys. Soc. $\underline{22}$, 1130 (1977).

2   D. J. Johnson, G. W. Kuswa, A. V. Farnsworth, Jr., J. P. Quintenz, et.al., Phys. Rev. Lett. $\underline{42}$, 610 (1979).

3   P. Dreike, C. Eichenberger, S. Humphries, and R. Sudan, J. Appl. Phys. $\underline{47}$, 85 (1976).

4   S. J. Stephanakis, J. R. Boller, G. Cooperstein, S. A. Goldstein, et.al., Bull. Am. Phys. Soc. $\underline{23}$, 907 (1978).

5   S. A. Goldstein and R. E. Lee, Phys. Rev. Lett. $\underline{35}$, 1079 (1975).

6   J. W. Shearer, Lawrence Livermore Lab Report UCRL-52129 (1976).

7   P. F. Ottinger, S. A. Goldstein, and D. Mosher, NRL Memo Report No. 4548 (1981).

8   D. G. Colombant, S. A. Goldstein, and D. Mosher, Phys. Rev. Lett. $\underline{45}$, 1253 (1980).

9   S. J. Stephanakis, J. R. Boller, G. Cooperstein, et. al., Bull. Am. Phys. Soc. $\underline{24}$, 1031 (1979).

10 R. A. Meger, F. C. Young, A. T. Drobot, et. al., NRL Memo Report 4477 (1981).

11 R. J. Barker, S. A. Goldstein, and A. T. Drobot, NRL Memo Report No. 4642 (1981).

12 R. J. Barker and S. A. Goldstein, to appear as a NRL Memo Report (1982).

13 Particle Beam Fusion Progress Report April 1978 through December 1978, Sandia National Labs, SAND 79-1011 (1979).

14 D. B. Seidel and J. P. VanDevender in Particle Beam Fusion Progress Report June 1979 - December 1979, Sandia National Labs, SAND 80-0974 (1980).

15 I. Langmuir and K. T. Compton, Rev. of Modern Physics $\underline{3}$, 191 (1931).

16 F. Friedlander, R. Hechtel, H. Jory, et.al., Megavolt-Megampere Electron Gun Study, DASA 2173, Varian Associates, Palo Alto, CA (1968).

17 Robert K. Parker, Technical Report AFWL-TR-73-92, U. S. Air Force Weapons Laboratory, Albuquerque, NM (1973).

18 K. D. Bergeron, Phys. Fluids $\underline{20}$, 693 (1977).

19 R. J. Barker, A. T. Drobot, R. E. Lee, and S. A. Goldstein, Proc. 9th Conf. on Numerical Simulation of Plasmas, Evanston, IL (1980).

20   R. J. Barker, Banach Center Publication $\underline{3}$, 255; Warsaw, Poland (1975).

21   B. L. Buzbee, F. W. Dorr, and J. A. George, Technical Report CS-71-195, Computer Science Dept., Stanford University, Stanford, CA (1971).

22   R. N. Sudan and R. V. Lovelace, Phys. Rev. Lett. $\underline{31}$, 1174 (1973).

23   R. V. Lovelace and E. Ott, Phys. Fluids $\underline{17}$, 1263 (1974).

24   A. Ron, A. A. Mondelli, and N. Rostoker, IEEE Trans. Plasma Science, $\underline{PS-1}$, 85 (1973).

25   R. J. Barker, S. A. Goldstein, and A. T. Drobot, IEEE Int. Conf. on Plasma Science, Madison, WI (1980).